Nested Switching Control Design for Fast PZT Actuated Nanopositioning

Jinchuan Zheng * Minyue Fu *

* School of Electrical Engineering and Computer Science, The University of Newcastle, Callaghan, NSW 2308, Australia (Tel: +61-02-49215963; e-mail: Jinchuan.Zheng@newcastle.edu.au; Minyue.Fu@newcastle.edu.au).

Abstract: This paper studies a new nested switching control (NSC) scheme for piezoelectric (PZT) actuators to achieve fast nanopositioning. Conventional PZT controllers typically neglect the actuator saturation nonlinearity for design simplicity but at the cost of reduced performance. By optimizing a quadratic performance cost function that explicitly involves the actuator saturation, the NSC can not only guarantee the system stability in the presence of saturation but also improve the tracking speed. The experimental results on an actual PZT nanopositioner show that the new control scheme has outperformed the conventional control by more than 12% in settling time within the full PZT operational range and with nanoscale precision.

1. INTRODUCTION

The piezoelectric (PZT) actuator is a well-known device for precision positioning and motion control. The PZT actuators have been widely used in a variety of applications such as optical trapping, biotechnology, and nanomanipulation (see e.g., Binnig et al. [1986], Yves [1995], and Zheng et al. [2008]). For long-range operations that require high precision, repeatability, and long-term stability, a servo controller is typically essential for the PZT actuator to eliminate the nonlinear hysteresis, creep effects, and vibrations. A thorough literature review on control approaches for PZT actuators is reported in Devasia et al. [2007]. In particular, for hysteresis and vibration compensations there are two main approaches: inversion-based feedforward Croft et al. [2001] and high-gain feedback Yi et al. [2009]. In the inversion-based feedforward approach, an accurate hysteresis and vibrational dynamic model is crucial for the effectiveness of the compensation because the desired output is fed through the inverse model to generate feedforward signals to cancel the hysteresis and vibrations. On the contrary, the high-gain feedback approach avoids the need for an accurate model. In such methods, hysteresis and vibrations are essentially regarded as input disturbances and the induced position error is detected by the position sensor and fed back to the controller to generate PZT control signals to correct for position errors.

Tracking control is another main control task for the PZT actuators, which aims to drive the position output to track a desired trajectory such as triangular waveforms in AFM applications Abramovitch et al. [2007] and step references in pick-and-place operations Yi et al. [2009]. To achieve these tasks, traditional proportional-integral-derivative (PID) controllers are generally used, see e.g., Yong et al. [2009]. Furthermore, advanced controllers designed with modern control technologies are also reported, see e.g., Devasia et al. [2007] and Zheng et al. [2008]. However, in most existing literature, the PZT actuator saturation nonlinearity is rarely explicitly considered in the

control design. Typically, due to the PZT actuator limited travel range, the control input should be constrained to avoid damage to the PZT ceramics. Nevertheless, most existing controllers are designed either by ignoring the saturation nonlinearity or by constraining the control input not to hit the saturation limit within the full PZT operating range. There are two main disadvantages of such control strategies, especially for step tracking control. The first one is that when the PZT actuator works around its maximum range, the performance may deteriorate (e.g., causing excessive oscillations) once large disturbance occurs because the control design does not guarantee fast convergence of the closed-loop system in the presence of saturation. The second one is that when the PZT actuator works in a small range, the allowable control input is not fully used thus, resulting in conservative performance (e.g., longer settling time). For these reasons, this paper proposes a novel control scheme that explicitly accounts for the saturation in the controller and leads to superiorly fast and precise step tracking performance.

The contribution of this paper lies in that we explicitly model the PZT actuator as a saturated actuator, for which the step tracking control problem is then casted as a linear quadratic control problem with input saturation. The solution of the problem eventually leads to a nested switching controller (NSC). Unlike the anti-windup compensator Kapoor et al. [1998] that uses ad-hoc methods to detune the controller with little theoretical guarantee on stability; or the control design to avoid the saturation at the cost of either reduced performance or shortened operational range, the proposed NSC not only guarantees the stability in the presence of saturation, but also optimizes a quadratic performance function through properly over-saturating the controller that leads to desired fast convergence of the tracking error.

This paper is organized as follows. Section 2 introduces the experimental setup and plant modeling of the PZT actuator nanopositioning system. Section 3 presents the
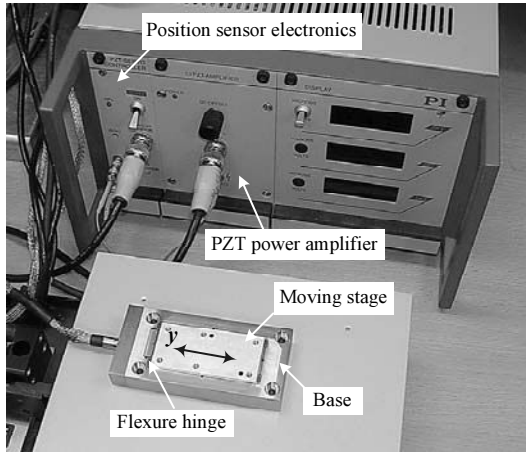
Fig. 1. Experimental setup of the PZT actuated nanopositioner (The PZT actuator/position sensor is attached to the moving stage and embedded into the base).

fundamental control theory of NSC design. Section 4 shows the experimental results of step tracking to demonstrate the effectiveness of the designed NSC controller. Section 5 concludes the paper.

2. PLANT MODELING

Fig. 1 shows the experimental setup of the PZT actuated nanopositioner (P-752, Polytec PI) studied in this paper. The nanopositioner comprises a flexure-guided moving stage that is driven by a PZT microactuator with a travel range of ± 12.5 μm, and a capacitive position sensor with a practical resolution of 14 nm to measure the displacement of the moving stage along the axis. The position sensor output is fedback to a real-time DSP system on which the feedback controller is implemented with the sampling frequency of 20 kHz. Subsequently, the control signal is passed through the power amplifier to output ten times voltage for the PZT actuator.

In real implementation, we have used an inner-loop precompensator to reduce the nonlinear hysteresis effects associated with the PZT and to damp the resonance modes of the flexure stage. We omit the detailed design and results here as it is not the main focus of this paper. Fig. 2 shows the frequency responses of the PZT actuator positioner with hysteresis and resonance compensation. The modeled PZT actuator plant model is given by

$$P = \frac{y}{\tilde{u}} = \frac{1}{(\tau_0 s + 1)^2 (\tau_1 s + 1)^3}, \quad (1)$$

where y is the controlled output displacement, $\tilde{u}$ the control input, $\tau_0 = 8.0 \times 10^{-4}$, and $\tau_1 = 3.2 \times 10^{-5}$.

3. NESTED SWITCHING CONTROL DESIGN

Our goal in this section is to find an optimal $\tilde{u}$ subject to the PZT input saturation such that the output displacement y can track any step reference input with amplitude y_r (within the PZT travel range) as fast as possible. In the following, we first formulate the PZT step tracking control problem as a standard regulation control problem; and then we introduce the fundamental theory of linear
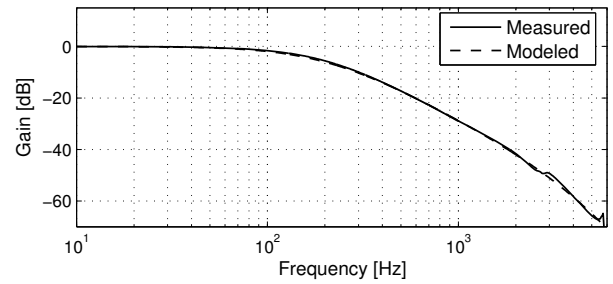

Fig. 2. Frequency responses of the PZT actuated nanopositioner with hysteresis and resonance precompensated.

quadratic (LQ) control with input saturation, based upon which a nested switching controller is developed to improve the tracking performance. Finally, we apply the switching control scheme to the PZT actuator and detail the design procedure. Experimental results are also presented to demonstrate the effectiveness of the developed controller.

3.1 Problem Formulation

Consider the system in (1) and let its state-space representation be given by

$$\begin{cases} \dot{x}_p = A x_p + \tilde{B} \sigma_p(\tilde{u}), & x_p(0) = x_{p0}, \\ y = C x_p, \end{cases} \quad (2)$$

where x_p is the state and the saturation function $\sigma_p(\tilde{u})$ defined as

$$\sigma_p(\tilde{u}) = \text{sgn}(\tilde{u}) \min\{\bar{u}, |\tilde{u}|\}, \quad (3)$$

where $\bar{u} = 12.5$ μm is the saturation level of the control input which, in our case, equals to the PZT maximum travel range.

The objective here is to design an optimal $\tilde{u}$ subject to the actuator saturation to cause the output y to track a step input y_r rapidly without experiencing large overshoot. Let

$$\tilde{u} = \sigma_s(u_s) + H y_r, \quad (4)$$

where y_r is the step input, u_s the control input to be designed as will be discussed later, H a scalar given by $H = -(CA^{-1}\tilde{B})^{-1}$ and $\sigma_s(\cdot)$ is defined as in (3) with the saturation level

$$\bar{u}_s = \bar{u} - |H y_r|, \quad (5)$$

where $|H y_r| \leq \bar{u}$. Note that here A is an asymptotically stable matrix and thus H is well defined. Furthermore, define x_r as $x_r := -A^{-1}\tilde{B}H y_r$ and let $x_e = x_p - x_r$, it is simple to transform (2) into

$$\dot{x}_e = A x_e + \tilde{B} \sigma_p(\tilde{u})$$
$$= A x_e + \tilde{B} \sigma_s(u_s) + A x_r + \tilde{B} H y_r + A^{-1}\tilde{B}H \dot{y}_r.$$

Noting that $A x_r + \tilde{B} H y_r + A^{-1}\tilde{B}H \dot{y}_r = 0$. Therefore, the closed-loop system is given by

$$\dot{x}_e = A x_e + \tilde{B} \sigma_s(u_s), \quad x_e(0) = x_{e0}. \quad (6)$$

To this end, we formulate the step tracking control design as a regulation control problem with input saturation. Next, we aim to find a state feedback control law u_s such that x_e converges to the origin rapidly. Once this is achieved, it indicates that $\lim_{t \to \infty} x_p(t) = x_r$. Therefore, $\lim_{t \to \infty} y(t) = C x_r = -CA^{-1}\tilde{B}H y_r = y_r$.

3.2 LQ Control with Input Saturation

Consider the system in (6). For the sake of easy presentation we replace the pair $(x_e, u_s, \tilde{B})$ with (x, u, B) and hence (6) can be rewritten as

$$\dot{x} = Ax + B\sigma(u), \quad x(0) = x_0, \tag{7}$$

where $x = x_e$, $B = \tilde{B}\bar{u}_s$, $u_s = u\bar{u}_s$ with $\bar{u}_s$ as (5), and $\sigma(\cdot)$ with saturation level equal to 1.

Next, we consider the following quadratic cost function

$$J(x_0, u) = \int_0^\infty (x^T \bar{Q} x + r\sigma(u)^2) dt \tag{8}$$

for some $\bar{Q} = \bar{Q}^T > 0$ and $r > 0$ with (A, B) being controllable. Ideally, we aim to seek an optimal linear state feedback $u = Kx$ for each given initial state x_0 such that $J(x_0, u)$ is minimized. It is well-known that if the control is not saturated, the optimal solution to K is given by

$$K = -r^{-1} B^T \bar{P}_0, \tag{9}$$

where $\bar{P}_0 = \bar{P}_0^T > 0$ is the solution to the following Ricatti equation

$$A^T \bar{P}_0 + \bar{P}_0 A + \bar{Q} - r^{-1} \bar{P}_0 BB^T \bar{P}_0 = 0. \tag{10}$$

Moreover, the minimal cost is given by $x_0^T \bar{P}_0 x_0$.

However, in the presence of saturation, the optimal K is difficult to give. To overcome this difficulty, we parameterize the controller by using an optimal sector bound Fu [2000]. More specifically, define the level of over-saturation $\rho \geq 0$ such that the control input u is restricted to be

$$|u| \leq 1 + \rho. \tag{11}$$

It is easy to verify that for any u constrained by (11), $\sigma(u)$ lies in the following sector bound

$$\sigma(u) = \rho_1 u + \delta(u), \tag{12}$$

$$|\delta(u)| \leq \rho_2 u, \quad \forall |u| \leq 1 + \rho, \tag{13}$$

where

$$\rho_1 = \frac{2 + \rho}{2(1 + \rho)}, \quad \rho_2 = \frac{\rho}{2(1 + \rho)}. \tag{14}$$

Here, ρ_1 is the optimal value so that $\delta(u)$ has the smallest sector to bound the nonlinearity cause by the saturation. This can be illustrated by Fig. 3.

Now, we give some analysis on the design of a control gain K to minimize the worst-case cost for all $\delta(\cdot)$ satisfying the sector bound (13). For a given $\rho > 0$, consider the Lyapunov function candidate

$$V(x) = x^T \bar{P}_\rho x, \quad \bar{P}_\rho = \bar{P}_\rho^T > 0, \tag{15}$$

and define

$$\Omega_\rho = A^T \bar{P}_\rho + \bar{P}_\rho A + \bar{Q} - r^{-1} \bar{P}_\rho BB^T \bar{P}_\rho, \tag{16}$$

$$u^* = -r^{-1} B^T \bar{P}_\rho x. \tag{17}$$

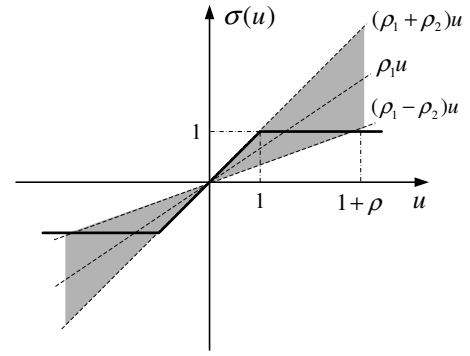Given any initial state x_0 and any $\delta(\cdot)$ satisfying (13), it is easy to verify that

Fig. 3. Illustration of sector bound for $\delta(u)$.

$$J(x_0, u, T) = V(x_0) - V(x(T))$$

$$+ \int_0^T (\frac{d}{dt} V(x) + x^T \bar{Q} x + r\sigma(u)^2) dt$$

$$\leq V(x_0) + \int_0^T f(x, u, \delta(u)) dt,$$

where

$$f(x, u, \delta(u)) = x^T \Omega_\rho x + r(\rho_1 u + \delta(u) - u^*)^2. \tag{18}$$

This implies that if $f(x, u, \delta(u)) \leq 0$ for all $x \in \mathbb{R}^n$ and $\delta(\cdot)$ satisfying (13), then

$$J(x_0, u) \leq V(x_0). \tag{19}$$

From the analysis above, we formulate the following relaxed optimal control problem:

P1: For a given $\rho \geq 0$, design $\bar{P}_\rho$ and u to minimize $V(x_0)$ subject to $f(x, u, \delta(u)) \leq 0$ for all $x \in \mathbb{R}^n$ and $\delta(\cdot)$ satisfying (13). Moreover, determine the largest invariant set X_ρ characterized by an ellipsoid of the form

$$X_\rho = \{x : x^T \bar{P}_\rho x \leq \mu_\rho^2\}, \quad \mu_\rho > 0, \tag{20}$$

such that if $x_0 \in X_\rho$, $x(t) \in X_\rho$ and $|u(t)| \leq 1 + \rho$ for all $t \geq 0$, we have $J(x_0, u) \leq V(x_0)$.

The solution to the above problem is given by the following Theorem:

Theorem 1 Fu [2000]: Consider the system in (7) and the cost function in (8). For a given level of over-saturation $\rho \geq 0$, suppose the equation

$$A^T \bar{P}_\rho + \bar{P}_\rho A + \bar{Q} - r^{-1}(1 - \rho_0^2) \bar{P}_\rho BB^T \bar{P}_\rho = 0, \tag{21}$$

where

$$\rho_0 = \frac{\rho_2}{\rho_1} = \frac{\rho}{2 + \rho} \tag{22}$$

has a solution $\bar{P}_\rho = \bar{P}_\rho^T > 0$. Then the optimal feedback control law K_ρ for the relaxed optimal control problem *P1* is given by

$$K_\rho = -\rho_1^{-1} r^{-1} B^T \bar{P}_\rho \tag{23}$$

and the associated invariant set X_ρ is bounded by

$$\mu_\rho = \frac{r}{(1 - \rho_0)\sqrt{B^T \bar{P}_\rho B}}. \tag{24}$$

Remark 1: If $\rho = 0$, the Riccati equation (21) and the control law (23) recover the results in (10) and (9) for optimal control without saturation. The associated invariant set is given by

$$X_0 = \{x : x^T \bar{P}_0 x \leq \mu_0^2\}, \quad \mu_0 = \frac{r}{\sqrt{B^T \bar{P}_0 B}}. \quad (25)$$

Remark 2: Despite that the invariant set enlarges when ρ increases, it can be seen that the upper bound of the performance cost in (19) becomes larger. This implies that the saturated controller can bring a good benefit when ρ is not close to 0 and not too large. Generally, ρ can be selected as the minimal one satisfying $x_0 \in X_\rho$.

Property of the control law   The proposed controller in Theorem 1 has two nice properties, i.e., the nesting property of X_ρ and monotonicity of $\bar{P}_\rho$. More specifically, define

$$S_\rho = (1 - \rho_0)\bar{P}_\rho. \quad (26)$$

We can rewrite the Riccati equation in (21) as

$$A^T S_\rho + S_\rho A + (1 - \rho_0)\bar{Q} - r^{-1}(1 + \rho_0)S_\rho BB^T S_\rho = 0 \quad (27)$$

and the invariant set can be expressed as

$$X_\rho = \{x : x^T S_\rho x \leq \frac{r^2}{B^T S_\rho B}\}. \quad (28)$$

Lemma 1 Fu [2000]: The solution S_ρ to (27) is monotonically decreasing in $\rho > 0$, i.e., for a sufficiently small $\epsilon > 0$, $S_\rho > S_{\rho+\epsilon}$, if $0 \leq \rho < \rho + \epsilon$. Consequently, X_ρ are nested in the following sense:

$$X_\rho \subset X_{\rho+\epsilon}, \quad \forall 0 \leq \rho < \rho + \epsilon. \quad (29)$$

Moreover, the solution $\bar{P}_\rho$ to the Riccata equation in (21) is monotonically increasing in $\rho > 0$. That is,

$$P_\rho < P_{\rho+\epsilon}, \quad \forall 0 \leq \rho < \rho + \epsilon. \quad (30)$$

3.3 Nested Switching Control

Thanks to the nesting property of X_ρ and monotonicity of $\bar{P}_\rho$, we can apply Theorem 1 to design a sequence of control gains K_i, based on which a nested switching control can be developed to improve the performance. More specifically, we choose a sequence of over-saturation bounds $0 = \rho_0 < \rho_1 < \cdots < \rho_N$ and solve the corresponding Lyapunov matrices $\bar{P}_i$, invariant sets X_i and controller gains K_i, $i = 0, 1, \cdots, N$. We then construct the nested switching control law by selecting the control gain K_i when $x \in X_i$ and $x \notin X_{i-1}$ (unless $i = 0$). The following result shows the advantage of the nested switching control in the performance improvement.

Lemma 2 Fu [2000]: Suppose the switching controller above is applied to the system in (7) with $x_0 \in X_N$, Let t_i be the time instance K_i is switched on, $i = 0, 1, \cdots, N$, particularly, $t_N = 0$. Then the cost of the switching control is bounded by

$$J(x_0, u) \leq x_0^T \bar{P}_N x_0 - \sum_{i=0}^{N-1} x^T(t_i)(\bar{P}_{i+1} - \bar{P}_i)x(t_i)$$

$$< x_0^T \bar{P}_N x_0. \quad (31)$$

From the theorem above, we can clearly see the advantage of the switching control by means of the negative term in (31) that decreases the cost gradually. In what follows, we will discuss how to choose $\bar{Q}$, r, and ρ_i and then apply the nested switching control to the PZT actuator for improved tracking performance.

3.4 Guidelines of Selecting $\bar{Q}$, r and ρ_i

Since the main purpose of using nested switching control is to speed up the transient response, it is intuitive to inject the maximum control input (by applying a large control gain K_i, $i > 0$) to achieve the fastest acceleration at the initial stage when the controlled output y is far away from the set point. When the controlled output y approaches the final set point, the control input should be gradually decreased (by applying a small control gain K_0) for a small overshoot. Such a control strategy would impose some conditions on $\bar{Q}$, r and ρ_i.

Firstly, we consider the controlled output y is close to the set point so as that the control gain K_0 (i.e., $\rho_0 = 0$) is applied. Under such a circumstance, the control input is not saturated. It is straightforward to verify that the closed-loop system can be expressed as

$$\dot{x} = (A - BB^T \bar{P}_0)x. \quad (32)$$

Clearly, we can select $\bar{Q}$ and r (hence corresponding to a unique solution of $\bar{P}_0$) such that the dominated poles of $A - BB^T \bar{P}_0$ should have a large damping ratio, which in turn will generate a small overshoot.

Secondly, to achieve a fast tracking speed when the controlled output y is far away from the set point, a larger control gain K_i corresponding to a $\rho_i > 0$ should take action prior to K_0. This implies that the associated invariant set X_0 as given by (25) should be as small as not to cover the initial state $x(0)$. Therefore, an additional stringent constraint is imposed on $\bar{Q}$ for such an X_0.

Last, for the given $\bar{Q}$ and r determined from above, according to Remark 3, choose ρ_N as the minimum satisfying $x(0) \in X_N(\rho_N)$. Subsequently, choose ρ_i with $0 < \rho_i < \rho_N$ provided that inserting the resulting K_i can bring further performance improvement (e.g., reducing steady-state chattering). Note that the control gain K_N associated with ρ_N will generally cause the control input to hit its saturation level at the initial stage for the purpose of maximum acceleration.

More specifically, the following procedure summarizes the guidelines for selecting $\bar{Q}$, r and ρ_i:

1) Without loss of generality, we set r as
$$r = 1 \quad (33)$$
since the performance cost can be normalized as J/r.

2) Given y_r and the resultant pair (A, B), select a $\bar{Q} = \bar{Q}^T > 0$ and solve (10) for a $\bar{P}_0$ such that the resulting closed-loop system matrix $A - BB^T \bar{P}_0$ has the desired poles locations, particularly, the dominated poles should have a large damping ratio. The solution of $\bar{P}_0$ can be easily obtained using the MATLAB command (`care`).

3) Calculate μ_0 using (25) and the initial state with
$$x(0) = x_{p0} - A^{-1}\tilde{B}(CA^{-1}\tilde{B})^{-1}y_r. \quad (34)$$

Check if $x(0)^T \bar{P}_0 x(0) > \mu_0^2$. If not, we go back to previous step and reselect $\bar{Q}$. Generally, increasing $\bar{Q}$ is effective due to the monotonicity property of the solution of the Riccati equation (10).

4) Solve $x(0)^T \bar{P}_N x(0) = \mu_N^2$ to yield ρ_N.

5) Evaluate the closed-loop performance by applying K_0 and K_N only (i.e, with the minimum switching controllers). If the control output y exhibits unacceptable overshoot or chattering in steady state, insert an interim controller K_i with $0 < \rho_i < \rho_N$ and so forth until the performance is acceptable.

3.5 Application to PZT Tracking Control

We consider an approximate second-order model of the PZT during the control design, which is given by

$$\dot{x}_p = \begin{bmatrix} 0 & 1 \\ a_1 & a_2 \end{bmatrix} x_p - \begin{bmatrix} 0 \\ \tilde{b} \end{bmatrix} \sigma_p(\tilde{u}), \quad x_p(0) = 0, \tag{35}$$
$$y = [\,1 \ 0\,] x_p,$$

where $x_p = [y \ \dot{y}]^T$, $a_1 = -1.1109 \times 10^6$, $a_2 = -1.9227 \times 10^3$, $\tilde{b} = 1.1409 \times 10^6$. We now follow the proposed procedure to design a nested switching controller for this system. In particular, for this simplified system, we can yield the controller analytically expressed by the design specifications for easy tuning of the performance. The design results are given as follows:

1) Let the desired poles for the closed-loop system matrix $A - BB^T \bar{P}_0$ be $(-\zeta \pm j\sqrt{1-\zeta^2})\omega$, where ζ represents the damping ratio and ω the natural frequency. We then parameterize $\bar{Q}$ as

$$\bar{Q} = \begin{bmatrix} q_1 & 0 \\ 0 & q_2 \end{bmatrix} \tag{36}$$

with

$$q_1 = \frac{1}{b^2}(\omega^4 - a_1^2), \tag{37}$$
$$q_2 = \frac{1}{b^2}(4\zeta^2\omega^2 - 2\omega^2 - 2a_1 - a_2^2), \tag{38}$$

where $b = \tilde{b}\bar{u}_s$. Clearly, to guarantee $\bar{Q} > 0$ requires ω and ζ satisfying the conditions

$$\omega > \sqrt{|a_1|}, \tag{39}$$
$$1 \geq \zeta^2 > \frac{(2a_1 + a_2^2)}{4\omega^2} + 0.5. \tag{40}$$

Substituting $\bar{Q}$ and $r = 1$ into (21) solves $\bar{P}_\rho$ as

$$\bar{P}_\rho = \begin{bmatrix} p_1 & p_2 \\ p_2 & p_3 \end{bmatrix} \tag{41}$$

with

$$p_1 = b^2(1 - \rho_0^2)p_2 p_3 - a_2 p_2 - a_1 p_3, \tag{42}$$
$$p_2 = \frac{a_1 + \sqrt{(1-\rho_0^2)\omega^4 - \rho_0^2 a_1^2}}{b^2(1 - \rho_0^2)}, \tag{43}$$
$$p_3 = \frac{a_2 + \sqrt{a_2^2 + b^2(1-\rho_0^2)(2p_2 + q_2)}}{b^2(1 - \rho_0^2)}. \tag{44}$$

Accordingly, the resulting control gain with respect to a given ρ is obtained by

$$K_\rho = -\frac{b}{\rho_1}[p_2 \ p_3]. \tag{45}$$

To this end, it is easy to verify that the closed-loop system characteristic polynomial for $\rho = 0$ is given by

$$\Delta_0(s) = |sI - A - BK_0|$$
$$= s^2 + (b^2 p_3 - a_2)s + (b^2 p_2 - a_1)$$
$$= s^2 + 2\zeta\omega s + \omega^2, \tag{46}$$

which yields the poles as specified initially.

2) According to (34) and (25), we can obtain

$$x(0) = [-y_r \ 0]^T, \tag{47}$$
$$\mu_0^2 = \frac{1}{a_2 + 2\zeta\omega}. \tag{48}$$

To satisfy $x(0)^T \bar{P}_0 x(0) > \mu_0^2$ is equivalent to that the following inequality

$$y_r^2(2\zeta\omega^3 - a_1 a_2) - b^2(a_2 + 2\zeta\omega)^{-1} > 0 \tag{49}$$

should hold. We have parameterized $\bar{Q}$ and K_ρ simply in terms of the design specifications ω and ζ with the basic selection criteria given in (39), (40) and (49). Generally, we can choose an initial ω and ζ satisfying (39)–(40) and check if (49) holds. If not, increase ω until (49) holds because of the monotonicity property of (49) with respect to ω. After that, we can finalize $\bar{Q}$ and seek the controllers with over-saturation in next step.

3) Choose ρ_N as the solution of ρ in the following equation

$$y_r = \frac{\rho + 2}{2b\sqrt{p_1 p_3}}, \tag{50}$$

where p_1 and p_3 are functions of ρ as given in (43) and (44), respectively. Note that such a ρ_N is unique since the right hand side of (50) is monotonically increasing with respect to ρ. We can easily achieve ρ_N using numerical methods.

We now follow the above procedure to find the NSC for the PZT actuator. We also define the *settling time* as the total time that it takes for the position output to enter and remain within ± 30 nm of the target set point. Note that as the adopted position sensor has a noise level of ± 14 nm, the specified position precision of 30 nm is almost the best achievable in practice.

We take the reference with $y_r = 500$ nm as an illustration example. After few iterations, we obtain $\omega = 2\pi 280$, $\zeta = 0.785$ and $\rho_1 = 13$. This leads to $q_1 = 9.9364$, $q_2 = 2.9 \times 10^{-8}$. We begin with using two switching controllers; hence, this leads to the controller gains

$$K_0 = -[2.141 \ \ 0.0009], \tag{51}$$
$$K_1 = -[5.6915 \ \ 0.0027], \tag{52}$$

and the corresponding Lyapunov matrices $\bar{P}_i$ and regions of attraction μ_i are respectively give by

$$\bar{P}_0 = \begin{bmatrix} 7.6286 \times 10^{-3} & 2.3457 \times 10^{-6} \\ 2.3457 \times 10^{-6} & 1.0076 \times 10^{-9} \end{bmatrix}, \quad \mu_0 = 0.0345,$$

$$\bar{P}_1 = \begin{bmatrix} 9.3673 \times 10^{-3} & 3.3405 \times 10^{-6} \\ 3.3405 \times 10^{-6} & 1.6059 \times 10^{-9} \end{bmatrix}, \quad \mu_1 = 0.205.$$
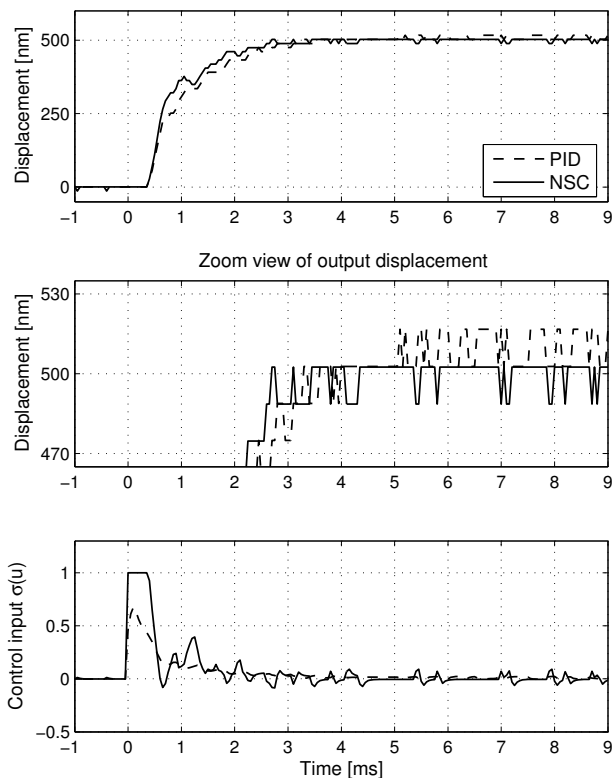
Fig. 4. Experimental step responses to $y_r = 500$ nm.

For comparison, we also design a PID controller as follows

$$u = \left(0.42 + \frac{17.5}{s} + \frac{7 \times 10^{-5}s}{6.36 \times 10^{-5}s + 1}\right)(y_r - y), \quad (53)$$

which can achieve the minimum settling time with non-saturated control input.

4. EXPERIMENTAL RESULTS

The NSC and PID controllers are implemented on the actual PZT nanopositioner. We use backward differentiation of the measurable position signals cascaded with an appropriate noise filter to estimate the velocity. The experimental results for the step response to $y_r = 500$ nm are shown in Fig. 4. We can see that compared with the PID, the NSC significantly reduces the settling time by properly over-saturating the control input. Moreover, we have also implemented other step responses with amplitudes over the full PZT travel range and found that the transient responses are similar with those in Fig. 4. We summarize all the results in terms of settling time in Table 1. It is clearly seen that the settling time under the NSC control is significantly reduced by more than 12% compared with the PID control. Finally, we need to emphasize that the controlled position precision (i.e., 30 nm) we achieved in this paper is almost the best in practice as the position sensor resolution is 14 nm in our setup. Provided that a position sensor of higher resolution is available, the proposed NSC control is also possible to provide further improvement on the control performance.

5. CONCLUSION

We have studied in this paper a new nested switching control scheme for the PZT actuator tracking control

Table 1. Comparison of the Settling time Improvement from experimental results

Step Length	Settling Time (ms)		Improvement
(nm)	PID	NSC	(%)
50	0.572	0.505	12
100	0.699	0.585	17
500	2.683	2.233	17
1000	3.14	2.625	17
3000	3.7	3.1	16
5000	3.71	3.08	17
8000	5.05	3.45	31
10000	5.065	3.49	31

with the actuator saturation nonlinearity explicitly taken into account. Distinct from the conventional control, the proposed control scheme can guarantee the closed-loop system stability in the presence of saturation, meanwhile significantly improve the tracking speed through switching the controllers that optimize a quadratic cost function. The experimental results demonstrate that the new control scheme has outperformed the conventional PID control by more than 12% in settling time within almost the full PZT operational range while nanoscale precision is maintained.

REFERENCES

G. Binnig, C. Quate, and C. Gerber, Atomic force microscope. *Phys. Rev. Lett.*, 56: 930-933, Mar. 1986.

M. Yves, *Scanning Probe Microscopes*, Bellingham, WA: SPIE, 1995.

J. Zheng, M. Fu, Y. Wang, and C. Du, Nonlinear tracking control for a hard disk drive dual-stage actuator system. *IEEE/ASME Trans. Mechatron.*, 13: 510-518, Oct. 2008.

S. Devasia, E. Eleftheriou, and R. Moheimani, A survey of control issues in nanopositioning. *IEEE Trans. Control Syst. Technol.*, 15: 802-823, Sep. 2007.

D. Croft, G. Shed, and S. Devasia, Creep, hysteresis, and vibration compensation for piezoactuators: atomic force microscopy application. *J. Dyn. Syst., Meas. Control*, 123: 35-43, Mar. 2001.

J. Yi, S. Chang, and T. Shen, Disturbance-observer-based hysteresis compensation for piezoelectric actuators. *IEEE/ASME Trans. Mechatron.*, 14: 456-464, Aug. 2009.

D. Abramovitch, S. Andersson, L. Pao, and G. Schitter, A tutorial on the mechanisms, dynamics, and control of atomic force microscopes. *Proc. Amer. Control Conf.*, 3488-2208, 2007.

Y. Yong, S. Aphale, and R. Moheimani, Design, identification, and control of a flexure-Based XY stage for fast nanoscale positioning. *IEEE Trans. Nanotechnol.*, 8: 46C54, Jan. 2009.

J. Zheng, Y. Guo, M. Fu, Y. Wang, and L. Xie, Development of an extended reset controller and its experimental demonstration. *IET Control Theory & Applications*, 2: 866-874, 2008.

N. Kapoor, A. Teel and P. Daoutidis, An anti-windup design for linear systems with input saturation. *Automatica*, 34: 559-574, 1998.

M. Fu, Linear quadratic control with input saturation. *Proc. Robust Control Workshop*, Newcastle, 2000.